

PCCP

Accepted Manuscript



This is an *Accepted Manuscript*, which has been through the Royal Society of Chemistry peer review process and has been accepted for publication.

Accepted Manuscripts are published online shortly after acceptance, before technical editing, formatting and proof reading. Using this free service, authors can make their results available to the community, in citable form, before we publish the edited article. We will replace this *Accepted Manuscript* with the edited and formatted *Advance Article* as soon as it is available.

You can find more information about *Accepted Manuscripts* in the [Information for Authors](#).

Please note that technical editing may introduce minor changes to the text and/or graphics, which may alter content. The journal's standard [Terms & Conditions](#) and the [Ethical guidelines](#) still apply. In no event shall the Royal Society of Chemistry be held responsible for any errors or omissions in this *Accepted Manuscript* or any consequences arising from the use of any information it contains.

Built-in potential shift and Schottky-barrier narrowing in organic solar cells with UV-sensitive electron transport layers

Cheng Li, Dan Credgington, Doo-Hyun Ko, Zhuxia Rong, Jianpu Wang^{1,a)} and Neil C. Greenham^{a)}

Cavendish Laboratory, JJ Thomson Avenue, Cambridge CB3 0HE, United Kingdom

Abstract

The performance of organic solar cells incorporating solution-processed titanium suboxide (TiO_x) as electron-collecting layers can be improved by UV illumination. We study the mechanism of this improvement using electrical measurements and electroabsorption spectroscopy. We propose a model in which UV illumination modifies the effective work function of the oxide layer through a significant increase in its free electron density. This leads to a dramatic improvement in device power conversion efficiency through several mechanisms - increasing in the built-in field by 0.3 V, increasing the conductivity of the TiO_x layer and narrowing the interfacial Schottky barrier between the suboxide and the underlying transparent electrode. This work highlights the importance of considering Fermi-level equilibration when designing multi-layer transparent electrodes.

¹ Present address: Jiangsu-Singapore Joint Research Center for Organic/Bio- Electronics & Information Displays and Institute of Advanced Materials(IAM), Nanjing Tech University, Nanjing 211816, China.

^{a)} Authors to whom correspondence should be addressed. Electronic addresses: iamjpwang@njtech.edu.cn or ncg11@cam.ac.uk.

Introduction

Organic photovoltaic (OPV) devices have attracted significant attention due to their potential to act as easy-to-process, large-area and flexible renewable energy sources.¹ To enhance the device power conversion efficiency (PCE) and stability, one emerging method is to insert buffer layers between the photoactive material and the electrodes, such as transition-metal oxides²⁻⁴ or water/alcohol-soluble conjugated polymers.^{5, 6} Although various methods have been applied to investigate the role of these buffer layers,⁷⁻¹⁰ the mechanism of the enhancement remains unclear.

One particularly promising buffer layer material is solution-processed titanium suboxide (TiO_x), which has been used as an electron transporting layer (ETL) in organic solar cells due to its ease of synthesis and deposition, and its role in enhancing device air stability.¹¹ While as-fabricated devices usually exhibit poor performance, this can be dramatically improved by UV illumination.^{12, 13} Although it is well known that the properties of the TiO_x layer will be significantly affected by exposure to UV light,¹⁴ detailed understanding of the correlation of OPV device performance with the TiO_x layer properties is still lacking. In order to study the role of the ETL layer in organic solar cells, here we utilize electroabsorption (EA) spectroscopy to investigate in-situ the change of built-in potential in the device upon UV illumination. We find that the built-in potential increases from 0.5 V to 0.8 V after UV exposure, which correlates with a significant improvement of device performance. We propose that this change is due to a decrease of the effective work function (the Fermi level moves towards the vacuum level) of the TiO_x layer which arises from a large increase in the density of mobile electrons within the TiO_x , narrowing the interfacial Schottky barrier with ITO and significantly reducing the associated contact resistance.

Experimental

We fabricated inverted OPV devices based on the model system of poly(3-hexylthiophene) (P3HT) blended with [6-6]-phenyl-C61-butyric acid methyl ester (PCBM), using TiO_x as the ETL. Figure 1(a) shows a schematic diagram of the device structure. Figure 1(b) shows the approximate energy level structure based on literature values.^{2, 15-17} Here the ITO layer acts as the electron-collecting electrode and Ag as the hole-collecting electrode. 20 nm thick amorphous TiO_x films were obtained by spin coating a precursor (titanium isopropoxide ($\text{Ti}[\text{OCH}(\text{CH}_3)_2]_4$)) on cleaned ITO substrates, followed by annealing at 150 °C for 1 h in air. The precursor solution was prepared as previously reported.¹² P3HT:PCBM (30 mg/ml, 1:0.8 by weight) dissolved in chlorobenzene was spin-cast onto the TiO_x layer in a nitrogen glove box. The resulting photoactive layer, with a thickness of ~100 nm, was annealed at 140 °C for 10 min under nitrogen. Thin films of MoO_3 (8 nm) and Ag (100 nm) were then deposited by vacuum evaporation (2×10^{-6} mbar). The overlap between ITO and Ag electrodes defined the effective device area of 1.5 mm².

The photovoltaic performance of the devices was characterized in air under simulated AM 1.5 G conditions at 100 mWcm⁻² (ABET Sun 2000) without encapsulation. A 380 nm UV cut-off filter was used to obtain the current-voltage (J-V) characteristics under visible illumination without significant excitation across the TiO_x bandgap. The filter was then removed to study the evolution of the device performance at 30 s intervals with the UV component restored (hereafter referred to as “UV illumination”).

Interfacial resistance was studied by fabricating electron-only devices with 100 nm thick evaporated Al electrodes deposited both directly onto TiO_x , and with a buffer layer of spin-cast PCBM, with a device area of 1 mm^2 . In-plane resistance was studied using thin films of TiO_x deposited onto insulating SiO_2 , with laterally spaced Al electrodes evaporated on top.

Results

Figure 2 shows the device PV performance before UV exposure and after various intervals of UV illumination. The initial device fill factor (FF) and external quantum efficiency (EQE) (shown in Figure 2(b)) are extremely poor, which result in a $<0.01\%$ power conversion efficiency before UV illumination, and open-circuit voltage (V_{OC}) is $\sim 0.50 \text{ V}$. With UV exposure, sequential measurements show device performance steadily improving. After $\sim 500 \text{ s}$ continuous UV illumination, the device performance saturates at a PCE of 3.1% , with short-circuit current (J_{SC}) of 9.7 mA/cm^2 , V_{OC} of 0.61 V and FF of 0.50 .

To examine the consequences of the UV treatment in thin films of TiO_x , we measured the resistance of electron-only devices comprising 20 nm of TiO_x deposited onto ITO and capped with 40 nm of spin-cast PCBM and evaporated Al. Figure 3(a) presents plots of resistance vs. voltage after different UV exposure doses. The TiO_x resistance decreases strongly with the bias, and as the UV dose increases. The resistance reaches a minimum at high forward bias, the value of which drops from $3 \times 10^5 \Omega$ before illumination to $6 \times 10^4 \Omega$ after UV illumination. We also measured devices omitting the PCBM layer (see supplementary information), but found that penetration of the TiO_x by evaporated Al led to significantly increased conductivity and shorting, although identical trends were observed upon UV illumination.

It has previously been shown that the resistance of TiO_x decreases after UV illumination.¹² Therefore, we first consider the possibility that this strong dependence of resistance on bias and UV exposure is governed by the change of *bulk* resistivity in the TiO_x layer alone. From in-plane resistivity measurements on TiO_x films, shown in Figure 3(b), we obtain a resistivity of $9 \times 10^3 \Omega \text{ m}$ before UV exposure, reducing to $1 \times 10^3 \Omega \text{ m}$ after exposure.¹⁸ We therefore expect the *bulk* resistivity of the 20 nm TiO_x ETL to only contribute 15-120 Ω to the device series resistance, depending on UV exposure, which will cause a negligible voltage drop for the current densities measured herein. In addition, a bias-independent bulk resistivity cannot reproduce the change in shape observed in the J-V curves measured for the photovoltaic device. We therefore rule out changes in bulk resistivity of the TiO_x layer as a direct contribution to the changes in device performance observed under UV illumination.

To investigate the origin of the observed changes in solar cell performance, we utilize electroabsorption spectroscopy to estimate the device built-in potential before and after UV illumination. EA is a non-invasive method which can probe the electric field distribution in organic light-emitting diodes^{19, 20} and solar cells.^{21, 22} Full experimental details are described elsewhere.²³ Briefly, we apply a bias to the device comprising a variable DC voltage (V_{DC}) and a small, fixed, AC modulation (V_{AC}). The superposition of built-in potential V_{BI} and the applied bias leads to a modulated internal electric field, causing a Stark shift of the semiconductor absorption. The electroabsorption spectrum is typically dominated by the first derivative of the absorption spectrum. By reflecting the monochromated probe light from the Ag electrode onto a silicon photodiode, the change in absorption is detected through a lock-in technique as a

modulation of the relative reflection coefficient, $\frac{\Delta R}{R}$. Assuming no injection of charge carriers into the device,²¹ the first harmonic electroabsorption signal is

$$\left. \frac{\Delta R}{R} \right|_{\omega} \propto \text{Im} \chi^{(3)}(h\nu)(V_{DC} - V_{BI})V_{AC} \sin(\omega t), \quad (1)$$

where $\text{Im} \chi^{(3)}(h\nu)$ is the imaginary part of the third-order susceptibility as a function of photon energy $h\nu$ and ω is the frequency of the AC modulation. If there is no significant charge accumulation in the film, i.e. the electrical field distribution in the photoactive layer is uniform, the built-in voltage V_{BI} will be given by the difference in work function between the two electrodes²⁴ and may be estimated from V_{null} , the value of V_{DC} for which the EA signal goes to zero.

Fig 4(a) shows an EA spectrum under -3 V DC bias and the first derivative of the absorption spectrum of a P3HT:PCBM thin film. The EA peak positions match well with the lineshape of the first derivative of the absorption spectrum. The agreement between these two spectra indicates that the EA signal originates primarily from the induced dipole moment in the P3HT:PCBM layer.²⁵ Note that there exists a difference between the two spectra, particularly at photon energies below 1.9 eV. This negative feature can be ascribed to the absorption of polarons doped into the P3HT by the MoO₃ contact.²⁶ In order to maximize the signal-to-noise ratio, we selected a photon energy of 2.0 eV to characterize the built-in potential of the device.

Figure 4(b) shows the DC bias dependence of the EA signal at 2.0 eV. Before UV illumination, the built-in potential in the device is 0.5 V, as estimated from V_{null} . This increases to 0.8 V after UV exposure. Note that under forward bias, the EA amplitude varies non-linearly with the voltage due to the increasing influence of excited-state bleaching and absorption from injected

charges.²⁷ After 12 h in the dark, V_{BI} returns to 0.5 V (see supplementary information), and the OPV performance of the device also reverts to that measured before UV illumination.

Discussion

We now discuss why TiO_x -based P3HT:PCBM solar cells respond so strongly to UV illumination, and how this is related to the observed changes in built-in field. The band diagrams of our device were simulated using PC1D software.²⁸ As illustrated in Figure 5(a), the built-in field is generated by the work function difference of the two oxide electrodes. Due to the high dielectric constants of MoO_3 ²⁹ and TiO_x ,³⁰ under reverse bias the electrical potential drops predominantly within the P3HT:PCBM layer. We estimate the work function of MoO_3 , which is insensitive to UV illumination,¹² to be 5.3 eV.³¹ The formation of a δ -hole layer between MoO_3 and the P3HT allows the formation of an ohmic contact, illustrated by the dipole layer Δ in Figure 5(a) and (b). Since V_{BI} before UV illumination is ~ 0.5 V, we obtain a work function of ~ 4.8 eV for TiO_x before UV illumination, which suggests the solution-deposited material contains a high density of sub-bandgap defects.² After UV illumination, V_{BI} increases to 0.8 V, meaning the TiO_x work function decreases to ~ 4.5 eV. Due to the energetic distribution of trap states in TiO_x showing exponential dependence on the energy, 1 order of magnitude increase of free charge carrier density using UV light can lead to 0.3 eV change of the Fermi level.³² This is consistent with the defect states being filled by photo-generated carriers, allowing the work function of TiO_x to move towards the conduction band at around 4.3 eV, as illustrated in figure 5(b).¹⁵ This is also consistent with our observation that the improved performance upon UV illumination is reversible, since the carriers trapped at defects will eventually de-trap and

recombine, returning the TiO_x to its original state. In addition, the increase in work function is consistent with the small increase in V_{OC} from ~ 0.50 V to 0.61 V. This indicates that before UV illumination, V_{OC} is limited by the work functions of the electrodes,³³ while after UV illumination the electron quasi-Fermi level is likely pinned to states in the PCBM.^{34, 35}

The modest increase in built-in potential cannot explain the marked increase in fill factor or J_{SC} upon UV illumination. To understand this, we must reconcile the differences in resistance measured in the lateral and sandwich structures. The modest drop in resistance in the lateral structure upon UV illumination corresponds to an increase in the free electron density of approximately one order of magnitude. The significantly different behaviour observed in the sandwich structures must therefore be dominated by contact effects. Upon deposition, the Fermi levels of the TiO_x and ITO equilibrate, necessitating electron transfer to the ITO and depleting the TiO_x film. This gives rise to a Schottky barrier between the ITO and TiO_x layers. An initial electron density of $\sim 10^{19} \text{ cm}^{-3}$ would lead to depletion widths of order 20-30 nm,³⁶ depending on the exact barrier height, rendering the TiO_x layer largely insulating and giving rise to a significant (and symmetric) tunnel barrier.³⁷ After UV exposure, the increase in electron density will reduce the depletion width sufficient to allow tunnelling through the Schottky barrier, such that the effective resistance approaches the bulk TiO_x . Again, this change is consistent with an order of magnitude increase in the free carrier density of the TiO_x . In the lateral structure on SiO_2 this effect does not occur, since little exchange of electrons is expected and any depletion at the contacts will be insignificant compared to the resistance of the channel between them.

The behaviour of the complete device is thus fully accounted for by these two effects, suggesting that it is the suppression of an interfacial Schottky barrier which facilitates extraction of photo-generated charge, reducing bimolecular recombination and leading to enhanced short-circuit current and improved fill factors.^{38, 39} We therefore also conclude that changes in trap-assisted recombination at the TiO_x interface play a relatively minor role in the change in device output.⁴⁰ ⁴¹ This is consistent with the traps being electrically inaccessible, which is implied by the very long “memory” of such TiO_x interlayers and our inability to reproduce the resistivity change by simply injecting carriers directly into the TiO_x .

In summary, we have investigated the role of TiO_x buffer layers in inverted P3HT:PCBM solar cells. We found that the improvement of device performance upon UV illumination arises from the increase in electron density within the TiO_x film as photogenerated carriers passivate deep traps. This increased electron density leads to a decrease in the work function of the TiO_x , a drop in its bulk resistivity and the narrowing of the Schottky barrier between the TiO_x and ITO. The drop in contact resistance due to TiO_x therefore leads to a significant increase in FF and J_{SC} , while the change in work function results in an increase in the built-in potential and a concomitant increase in V_{OC} . These observations are important not only for OPV devices with TiO_x electron transport layers, but also for other interlayer systems requiring significant charge transfer to achieve equilibrium. In particular, while the work function modification accomplished by depositing TiO_x on ITO is crucial for achieving inverted devices, the significant electronic rearrangement and resulting depletion of the TiO_x may be detrimental. This suggests that transparent electrodes with a lower work function than ITO may be better paired with TiO_x in

stable inverted devices, and explains why such effects are rarely observed when TiO_x is used as an electron-collecting buffer layer underneath a lower work function metal such as Al.³⁷

Acknowledgements

We are grateful to Y. Vaynzof, O. Pachoumi, A. Chepelianskii and K. Musselman for valuable discussions, and to EPSRC via the SUPERGEN Excitonic Solar Cells Consortium [Grant number EP/G031088/1] for financial support. C. L. acknowledges the Chinese Scholarship Council and D. C. acknowledges Cambridge Display Technology for funding.

References:

1. K. M. Coakley and M. D. McGehee, *Chem. Mater.*, 2004, **16**, 4533.
2. J. Y. Kim, S. H. Kim, H.-H. Lee, K. Lee, W. Ma, X. Gong and A. J. Heeger, *Adv. Mater.*, 2006, **18**, 572.
3. B. V. Andersson, D. M. Huang, A. J. Moulé and O. Inganäs, *Appl. Phys. Lett.*, 2009, **94**, 043302.
4. M. T. Greiner, M. G. Helander, W.-M. Tang, Z.-B. Wang, J. Qiu and Z.-H. Lu, *Nat. Mater.*, 2012, **11**, 76.
5. Z. He, C. Zhong, X. Huang, W.-Y. Wong, H. Wu, L. Chen, S. Su and Y. Cao, *Adv. Mater.*, 2011, **23**, 4636.
6. Z. He, C. Zhong, S. Su, M. Xu, H. Wu and Y. Cao, *Nat. Photonics*, 2012, **6**, 591.
7. J. Kong, J. Lee, Y. Jeong, M. Kim, S.-O. Kang and K. Lee, *Appl. Phys. Lett.*, 2012, **100**, 213305.
8. Y. Vaynzof, A. Bakulin, S. Gélinas and R. H. Friend, *Phys. Rev. Lett.*, 2012, **108**, 246605.
9. T. Kuwabara, C. Iwata, T. Yamaguchi and K. Takahashi, *ACS Appl. Mater. Interfaces*, 2010, **2**, 2254.
10. H. Kim, J. Hwa Seo and S. Cho, *Appl. Phys. Lett.*, 2011, **99**, 213302.
11. J. Li, S. Kim, S. Edington, J. Nedy, S. Cho, K. Lee, A. J. Heeger, M. C. Gupta and J. T. Yates Jr, *Sol. Energy Mater. Sol. Cells*, 2011, **95**, 1123.
12. D.-H. Ko, J. R. Tumbleston, M.-R. Ok, H. Chun, R. Lopez and E. Samulski, *J. Appl. Phys.*, 2010, **108**, 083101.
13. D. Credginton, R. Hamilton, P. Atienzar, J. Nelson and J. R. Durrant, *Adv. Funct. Mater.*, 2011, **21**, 2744.
14. K. Sakaguchi, K. Shimakawa and Y. Hatanaka, *Phys. Status Solidi C*, 2011, **8**, 2796.
15. J. H. Lee, S. Cho, A. Roy, H.-T. Jung and A. J. Heeger, *Appl. Phys. Lett.*, 2010, **96**, 163303.

16. Y. Vaynzof, D. Kabra, L. Zhao, L. L. Chua, U. Steiner and R. H. Friend, *ACS Nano*, 2011, **5**, 329-336.
17. K. J. Reynolds, J. A. Barker, N. C. Greenham, R. H. Friend and G. L. Frey, *J. Appl. Phys.*, 2002, **92**, 7556.
18. B. Nasr, S. Dasgupta, D. Wang, N. Mechau, R. Kruk and H. Hahn, *J. Appl. Phys.*, 2010, **108**, 103721.
19. J. C. deMello, J. J. Halls, S. C. Graham, N. Tessler and R. H. Friend, *Phys. Rev. Lett.*, 2000, **85**, 421.
20. P. A. Lane, S. Chen and F. So, *J. Photon. Energy.*, 2011, **1**, 011020.
21. T. Drori, J. Holt and Z. Vardeny, *Phys. Rev. B*, 2010, **82**, 075207.
22. I. Hiromitsu, Y. Murakami and T. Ito, *J. Appl. Phys.*, 2003, **94**, 2434.
23. T. M. Brown, R. H. Friend, I. S. Millard, D. J. Lacey, T. Butler, J. H. Burroughes and F. Cacialli, *J. Appl. Phys.*, 2003, **93**, 6159.
24. I. H. Campbell, T. W. Hagler, D. I. Smith and J. P. Ferraris, *Phys. Rev. Lett.*, 1996, **76**, 1900.
25. F. W. Vance, R. D. Williams and J. T. Hupp, *Int. Rev. Phys. Chem.*, 1998, **17**, 307.
26. M. Zhou, L.-L. Chua, R.-Q. Png, C.-K. Yong, S. Sivaramakrishnan, P.-J. Chia, A. T. S. Wee, R. H. Friend and P. K. H. Ho, *Phys. Rev. Lett.*, 2009, **103**, 036601.
27. P. J. Brewer, P. A. Lane, A. J. DeMello, D. D. C. Bradley and J. C. DeMello, *Adv. Funct. Mater.*, 2004, **14**, 562.
28. UNSW PCID, <http://www.engineering.unsw.edu.au/energy-engineering/pcid-software-for-modelling-a-solar-cell>.
29. M. Sayer, A. Mansingh, J. B. Webb and J. Noad, *J. Phys. C: Solid State Phys.*, 1978, **11**, 315.
30. R. B. van Dover, *Appl. Phys. Lett.*, 1999, **74**, 3041.
31. V. Shrotriya, G. Li, Y. Yao, C.-W. Chu and Y. Yang, *Appl. Phys. Lett.*, 2006, **88**, 073508.
32. P. R. F. Barnes, A. Y. Anderson, J. R. Durrant and B. C. O'Regan, *Phys. Chem. Chem. Phys.*, 2011, **13**, 5798.
33. V. D. Mihailetschi, P. W. M. Blom, J. C. Hummelen and M. T. Rispens, *J. Appl. Phys.*, 2003, **94**, 6849-6854.
34. S. Braun, W. R. Salaneck and M. Fahlman, *Adv. Mater.*, 2009, **21**, 1450.
35. S. Cho, J. H. Seo, K. Lee and A. J. Heeger, *Adv. Funct. Mater.*, 2009, **19**, 1459.
36. L. Kavan and M. Graetzel, *Electrochimica Acta*, 1995, **40**, 643.
37. J. H. Seo, H. Kim and S. Cho, *Phys. Chem. Chem. Phys.*, 2012, **14**, 4062.
38. F. Etzold, I. A. Howard, R. Mauer, M. Meister, T.-D. Kim, K.-S. Lee, N. S. Baek and F. Laquai, *J. Am. Chem. Soc.*, 2011, **133**, 9469.
39. C. G. Shuttle, R. Hamilton, B. C. O'Regan, J. Nelson and J. R. Durrant, *Proc. Natl. Acad. Sci. USA.*, 2010, **107**, 16448.
40. Y. Liu, S. R. Scully, M. D. McGehee, J. Liu, C. K. Luscombe, J. M. J. Fréchet, S. E. Shaheen and D. S. Ginley, *J. Phys. Chem. B*, 2006, **110**, 3257.
41. Y.-J. Kang, C. Su Kim, D. Sung You, S. Hoon Jung, K. Lim, D.-G. Kim, J.-K. Kim, S. Hyung Kim, Y.-R. Shin, S.-H. Kwon and J.-W. Kang, *Appl. Phys. Lett.*, 2011, **99**, 073308.

Figure captions:

FIG. 1. a) Device structure of a bulk heterojunction inverted organic solar cell, using TiO_x as the electron transport layer. b) Energy level diagram of the OPV device.

FIG. 2. a) J-V curves for the complete device, before and during exposure to UV light, at 30 s intervals. J-V curves on a logarithmic scale, taken before and after UV illumination, are shown in the inset. b) EQE spectrum taken before and after UV illumination. The EQE amplitude before UV illumination is multiplied by 50 for clarity.

FIG. 3. a) Resistance-voltage curve for Al/PCBM/ TiO_x /ITO glass sandwich structure before and after 30 min UV illumination. The inset shows a schematic diagram of the structure, which has an active area of 1 mm^2 . b) Current-voltage measurement for a TiO_x thin film on a Si/ SiO_2 substrate with laterally spaced Al electrodes, before and after 30 min UV illumination. Channel length $L=20 \text{ }\mu\text{m}$, channel width $W=1 \text{ mm}$. The inset shows a schematic diagram of the structure.

FIG. 4. a) Electroabsorption spectrum under -3V external DC voltage (black), and first derivative of absorption spectrum of P3HT:PCBM (red). b) The DC bias dependence of the EA signal at 2.0 eV , taken before and after UV illumination.

FIG 5. Schematic energy diagrams for the device. a) Before UV exposure and b) after UV exposure. Δ represents the dipole layer due to a formation of a δ -hole layer between P3HT:PCBM and MoO_3 .

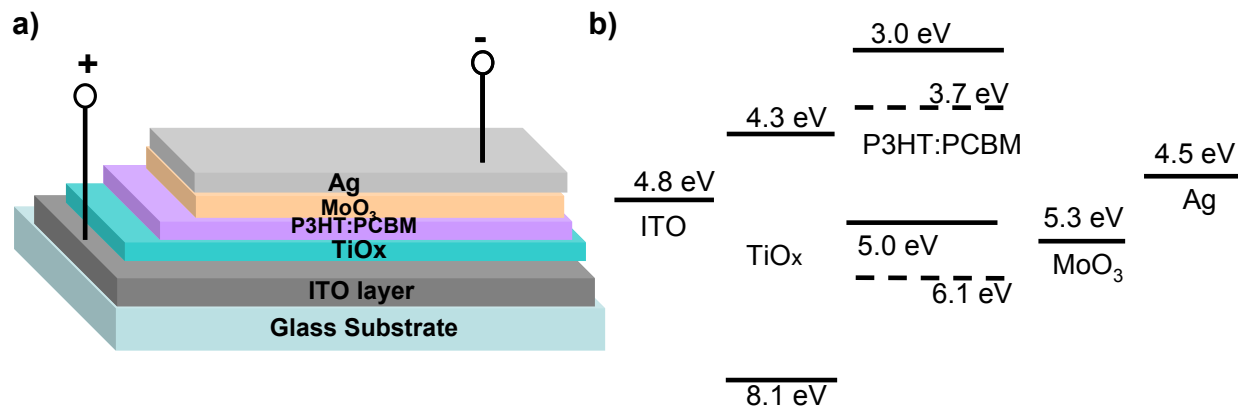


Figure 1.

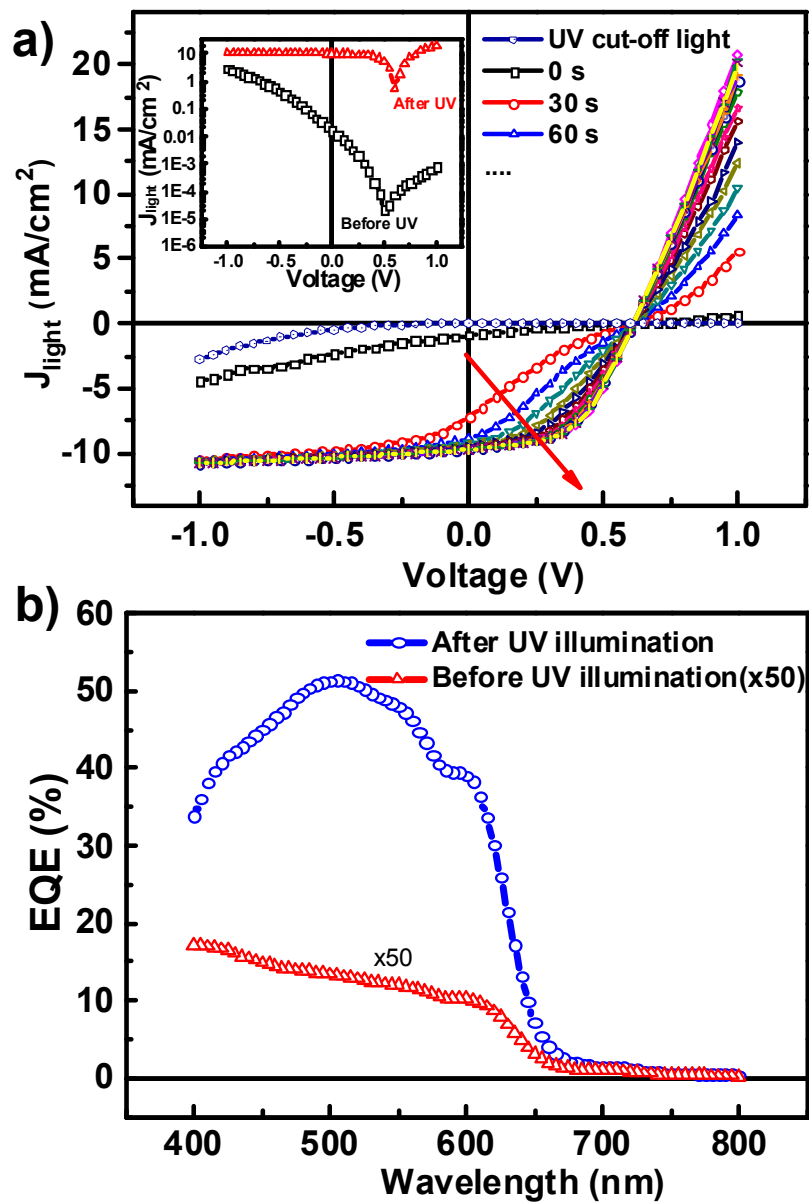


Figure 2.

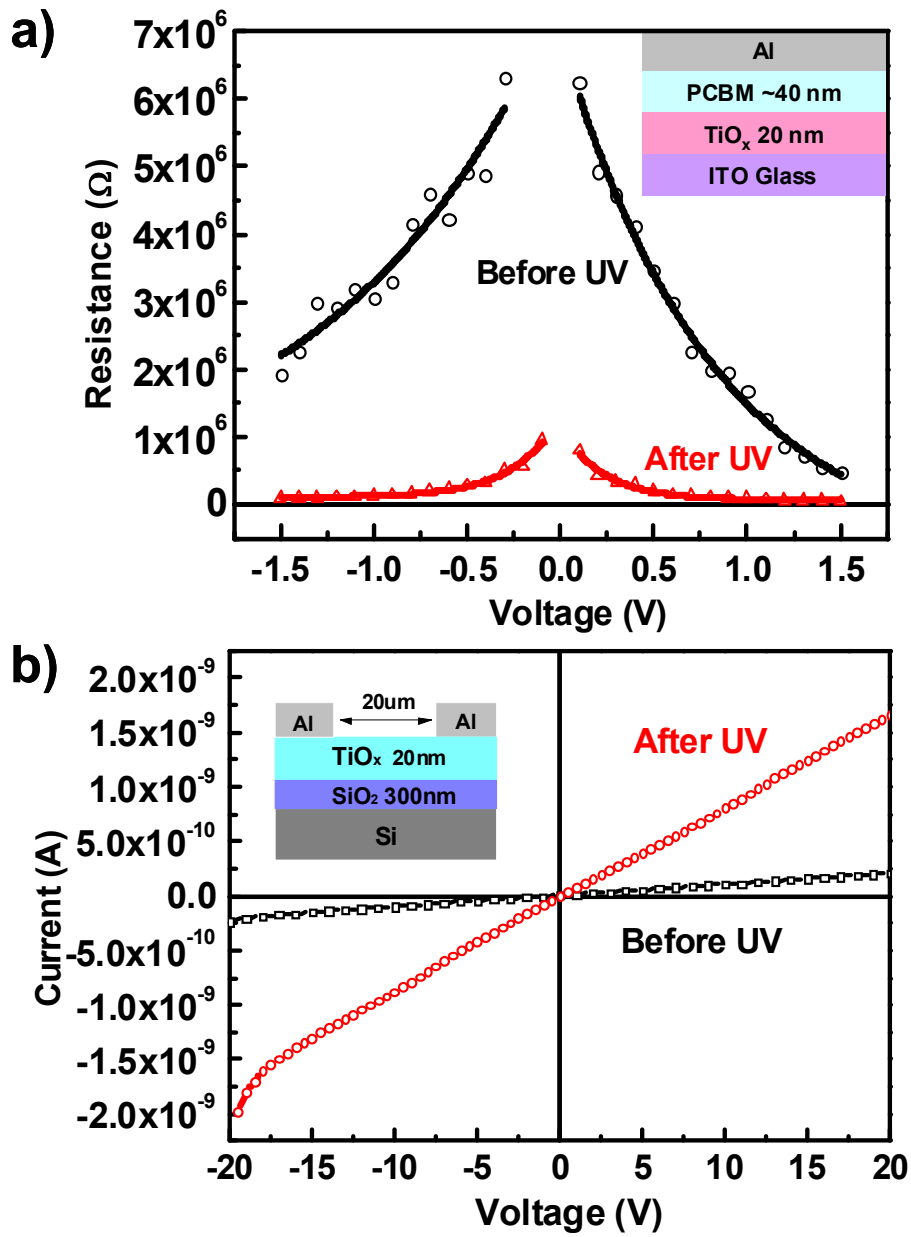


Figure 3.

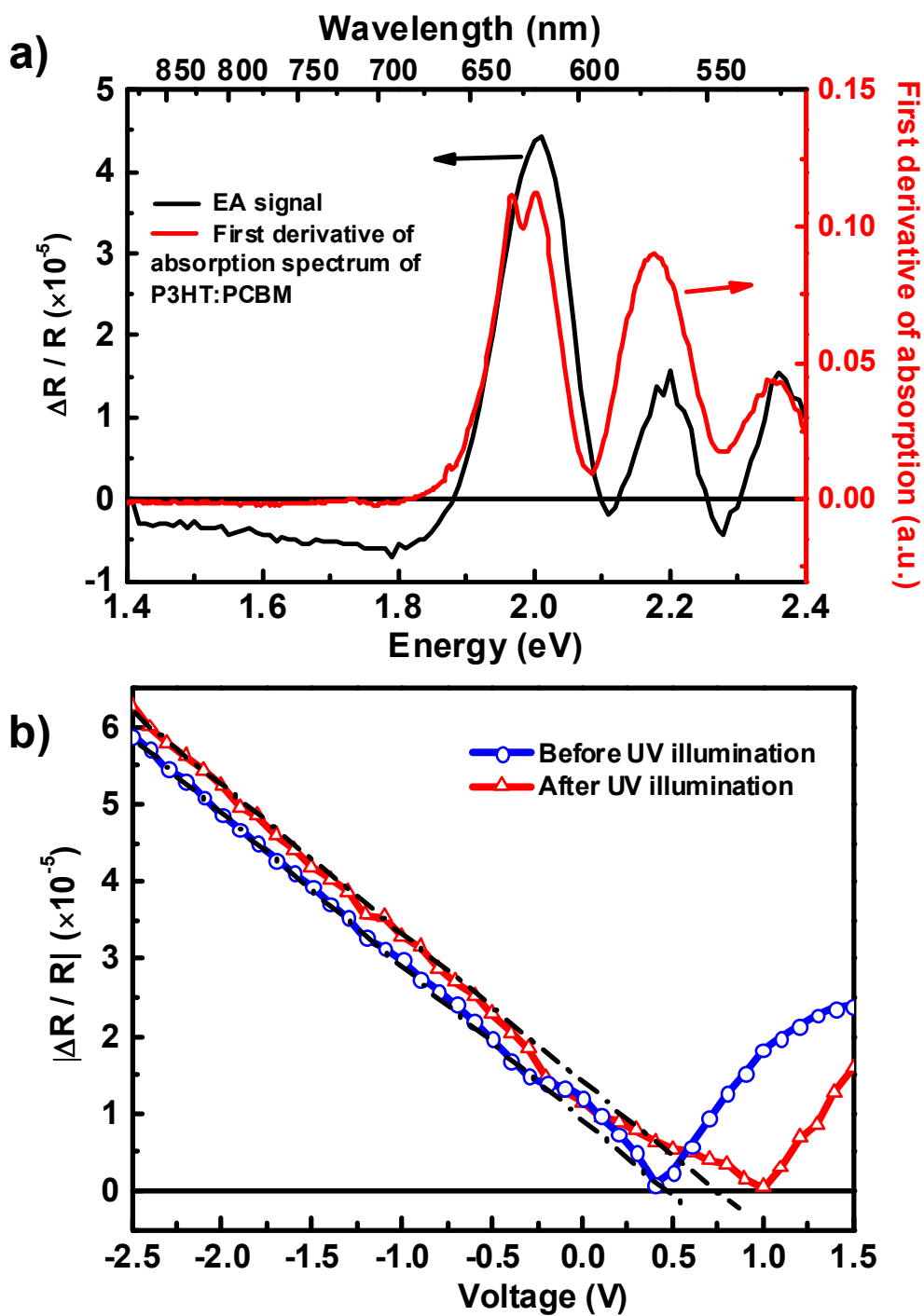


Figure 4.

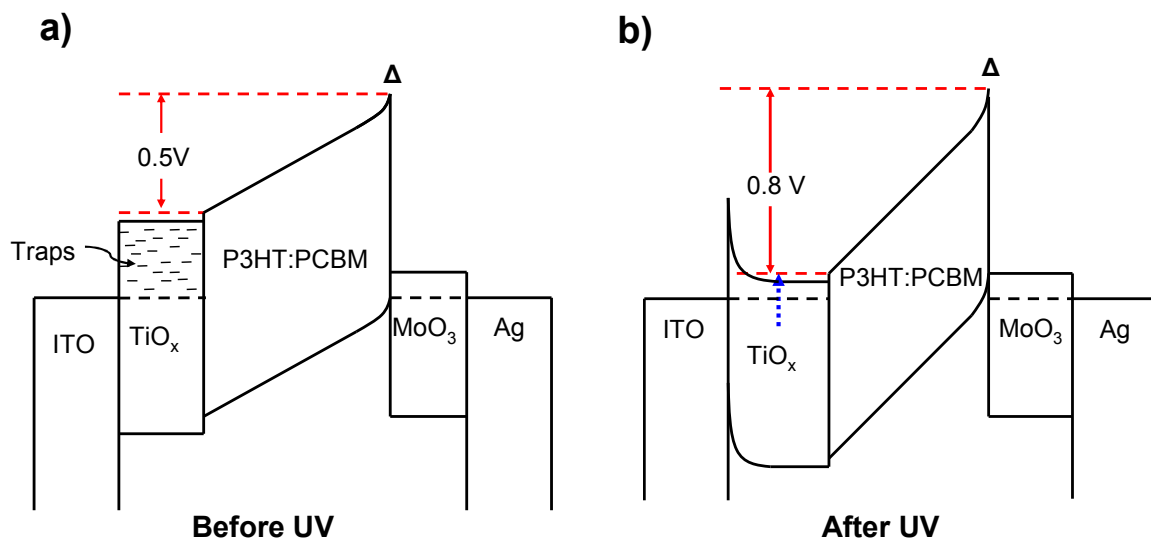


Figure 5.